molecules

MDPI

Article

Ru-Based NSAIDs as Potential Anticancer Therapeutics

Silvia Bordoni [1,*], Magda Monari [2], Carla Boga [1,*], Federico Moro [1] and Giacomo Drius [1]

[1] Department of Industrial Chemistry 'Toso Montanari', Alma Mater Studiorum, Università di Bologna, Via Piero Gobetti, 85, 40129 Bologna, Italy; federico.moro2@studio.unibo.it (F.M.); giacomo.drius2@unibo.it (G.D.)
[2] Department of Chemistry 'Giacomo Ciamician', Alma Mater Studiorum, Università di Bologna, Via Piero Gobetti, 85, 40129 Bologna, Italy; magda.monari@unibo.it
* Correspondence: silvia.bordoni@unibo.it (S.B.); carla.boga@unibo.it (C.B.)

Abstract

The use of metal-based species bearing existing pharmaceuticals as ligands—often resulting in enhanced bioactivity—represents an attractive strategy for the development of novel therapeutic formulations. In this context, five well-known non-steroidal anti-inflammatory drugs (NSAIDs) were employed to substitute both PPh_3 and hydride ligands in $[Ru(H)_2(CO)(PPh_3)_3]$ (**1**), thereby selectively affording neutral κ^2-(O,O)–chelate complexes in satisfactory yields via molecular hydrogen release. Among the obtained species, two complexes coordinating diclofenac (**4**) and aspirin (**5**) were further investigated by single-crystal X-ray diffraction (SCXRD). Preliminary biological studies were conducted on the ruthenium–salicylic acid species **2** and ibuprofen **6**. The former showed promising antiproliferative activity against HeLa cancer cells, consistent with the well-established role of NSAID–ruthenium(II) complexes as a platform for the development of novel anticancer metallotherapeutics.

Keywords: metallo-prodrugs; ruthenium; SCXRD; cancer

1. Introduction

The increasing societal impact of cancer has prompted the scientific community to seek novel chemotherapeutic agents with reduced side effects. The search for novel and effective anticancer agents has fuelled a growing interest in the development of transition metal complexes encompassing biologically relevant molecules. Metal-based species containing versatile ruthenium coordinated to multi-functionalized ligands undoubtedly occupy a prominent position in this field [1–6]. Non-steroidal anti-inflammatory drugs (NSAIDs) constitute a well-known, broad class of medications used to treat pain and inflammation and exhibit similar pharmacological properties, mechanisms of action, and side effects [7]. These compounds possess a variety of biological activities due to their ability to bind plasma proteins, a feature primarily ascribed to amphiphilic properties. Their structure includes hydrophilic groups, such as carboxyl or enol functions, together with lipophilic groups, such as aromatic rings or halide units [8,9].

Cyclooxygenase enzymes are known to play a crucial role in inflammation and carcinogenesis by catalyzing the conversion of arachidonic acid into prostaglandins [10]. NSAIDs have been demonstrated to reduce the incidence of several cancers, including breast, lung, and colorectal [11], through non-selective inhibition of cyclooxygenase-1 (COX-1), cyclooxygenase-2 (COX-2), and lipoxygenase (LOX) metabolism, which plays a significant role in angiogenesis by promoting migration of endothelial cells [12].

Academic Editors: Roxana Liana Lucaciu and Adriana Corina Hangan

Received: 15 January 2026
Revised: 29 January 2026
Accepted: 30 January 2026
Published: 9 February 2026

In recent decades, multiple studies have demonstrated the existence of a strong correlation between inflammation and cancer development. A combinatory action, ascribable to the synergistic therapeutic effects arising from the combination of anti-inflammatory properties with Ru-based anticancer activities, has been recently demonstrated to be more than mere speculation [13,14]. NSAID–ruthenium (II) complexes represent a promising area of research in the development of novel anticancer treatments that leverage the combined benefits of anti-inflammatory and anticancer effects. In fact, this dual functionality (Ru site and NSAID) offers an alternative approach, targeting both inflammation and neoplastic growth and, in certain cases, improving efficacy and selectivity compared with fragments alone. Recently, Martling's group reported a remarkable result, relating low-dose aspirin to the control of localized colorectal cancer [15]. It is noteworthy that aspirin, as an anti-inflammatory molecule, can also exhibit anticancer activity alone. In the case of the Ru-coordinating species **5,** this aptitude is expected to be enhanced, according to the trend of analogous Ru compounds. These types of organo–inorganic systems are reported to exhibit advantages by enhancing therapeutic value by the combined ability of anti-inflammatory features with Ru-anticancer potential [16]. Sáez's group reported that the presence of PPh_3 moieties induces intercalation reactions with DNA [17].

The presence of the metal is crucial and implies several accessible and stable oxidation states under physiological conditions. The Ru site acts as a carrier species due to its analogue Fe redox potentials and its affinity for Fe–transferrin, thereby slowing ligand exchange in vivo and allowing greater chemotherapeutic durability and improved drug internalization. The iron-mimicking ability to bind specific proteins, such as albumin, results in higher accumulation of ruthenium inside tumor cells compared to healthy cells. [18–22]. The biological responses are indeed attributable to the synergistic effects of the metal ion core interacting with NSAID pharmacophores [10]. Several studies have reported the success of [Ru(η^6-p-cymene)(NSAID)Cl], which coordinates ibuprofen, aspirin, naproxen, and diclofenac as k^2-(O,O)-chelate ligands (Figure 1) [21,23]. The obtained complexes demonstrate significant antiproliferative activity against different cancer cell lines.

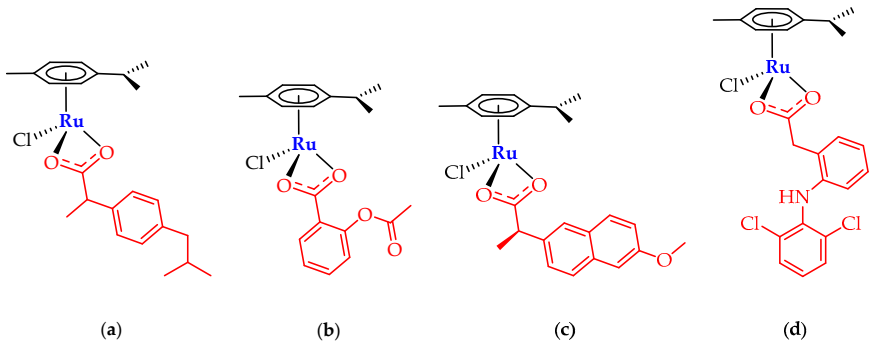

Figure 1. Piano stool [Ru(η^6-p-cymene)(NSAID)Cl] complexes with (**a**) ibuprofen, (**b**) aspirin, (**c**) naproxen, and (**d**) diclofenac; Mandal (2018) [21].

The above class of Ru complexes demonstrates promising antiproliferative activity against various cancer cell lines, such as cervical (HeLa), breast (MCF-7), and lung (A549), as well as tumors, with growth-inhibition values comparable to those of the most efficient current antineoplastic drugs [23]. The results reported from other authors for similar phosphine compounds indicate higher activity, corresponding to a lower dose (IC_{50}) for fighting cancer cells. Specifically, Graminha (2022) indicated 3.46 μM for [Ru(dppe)$_2$(A)] (Figure 2a), compared to the 8.91 μM for *cis*-platin on the MCF-7 breast cancer cell line, while Correa (2025) reported a value of 0.66 μM for [Ru(bipy)(dppp)(A)] (Figure 2b) compared with 11.80 μM for *cis*-Pt on the A2780 ovarian cell line [24–27].

Further, the cyclometalated Ru complex [Ru(CCC-Nap)(Ibu)(PTA)] (Figure 2c), concomitantly incorporating ibuprofen and naproxen-derived ligand, displays significant cancer cell cytotoxicity [28–30]. The structural similarity to the *trans*-phosphines complexes described by Correa—[Ru(PPh_3)$_2$(Th)(bipy)]PF_6, in which Th indicates thiourea derivatives [31]—and by Baratta's group—[Ru(OAc)(acac)(PPh_3)$_2$] [32]—has prompted the assumption of analogous amphiphilic properties for our class of metal systems.

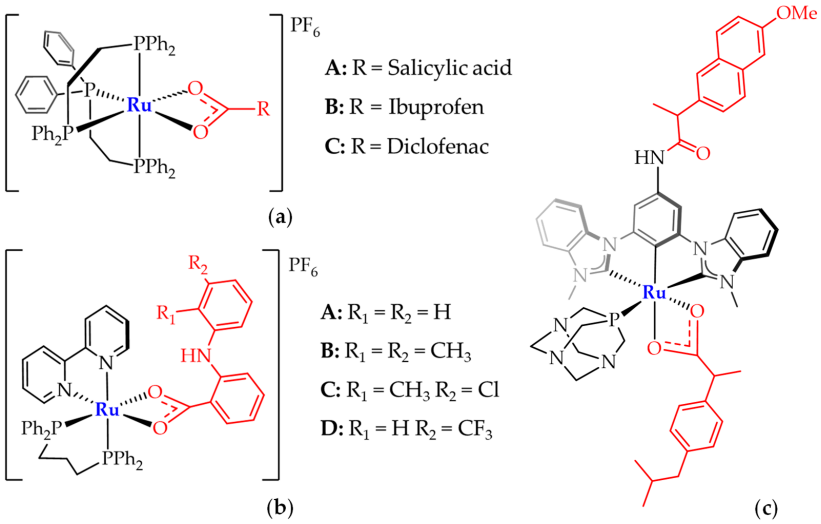

Figure 2. Ruthenium–NSAID complexes encompassing phosphine ligands. (**a**) Graminha (2022) [25], (**b**) Correa (2025) [27], (**c**) Tabrizi (2019) [30].

In the present report, we described the chemistry of five different NSAIDs (salicylic acid **2**, naproxen **3**, diclofenac **4**, acetylsalicylic acid **5**, and ibuprofen **6**) with the ruthenium hydride precursor [Ru(H)$_2$(CO)(PPh_3)$_3$] **1**, achieving the correspondent adducts [RuH(CO)(PPh_3)$_2$(NSAID)] by thermal solicitation in satisfactory yields. The selected NSAIDs span a broad range of polarities, as reflected by their log *p* values (salicylic acid/acetylsalicylic acid ≈ 1.1 < naproxen ≈ 3.2 < ibuprofen ≈ 4.0 < diclofenac ≈ 4.5), as shown in Figure 3. Variations in ligand polarity may influence the physical–chemical properties of the corresponding Ru–NSAID complexes, potentially affecting cellular uptake and intracellular distribution.

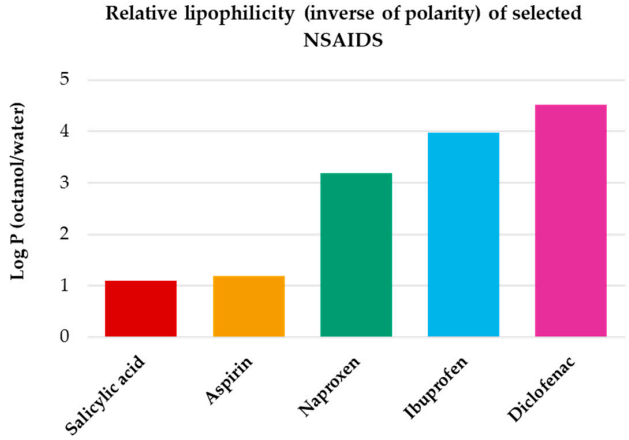

Figure 3. Diagram correlating polarity features of the selected NSAIDs expressed by water/octanol partition coefficient (logarithmic scale). Log$P_{O/W}$: salicylic acid = 1.09; aspirin = 1.19; naproxen = 3.18; ibuprofen = 3.97; diclofenac = 4.51. Data from Scott (2002), Krishnamoorti (2010), Brandenburg (2016), and the MolMeDB Database [33–36].

2. Results and Discussion

Complexes of the general formula [RuH(CO)(PPh_3)$_2$(NSAID)] were obtained in a 49–79% range by the reaction of the parent compound (**1**) [Ru(H)$_2$(CO)(PPh_3)$_3$] with a slight excess of the NSAID to obtain the expected Ru(II)–NSAID complexes as unique species via selective H_2 release and elimination of a PPh_3 ligand. All the synthesized complexes were treated with Et_2O extractions and recrystallized. Their proposed structures were supported by analytical and spectroscopic data, including ESI-MS, FTIR, ^{1}H, ^{31}P{^{1}H}, ^{13}C{^{1}H} NMR, and UV–Vis spectra (Scheme 1).

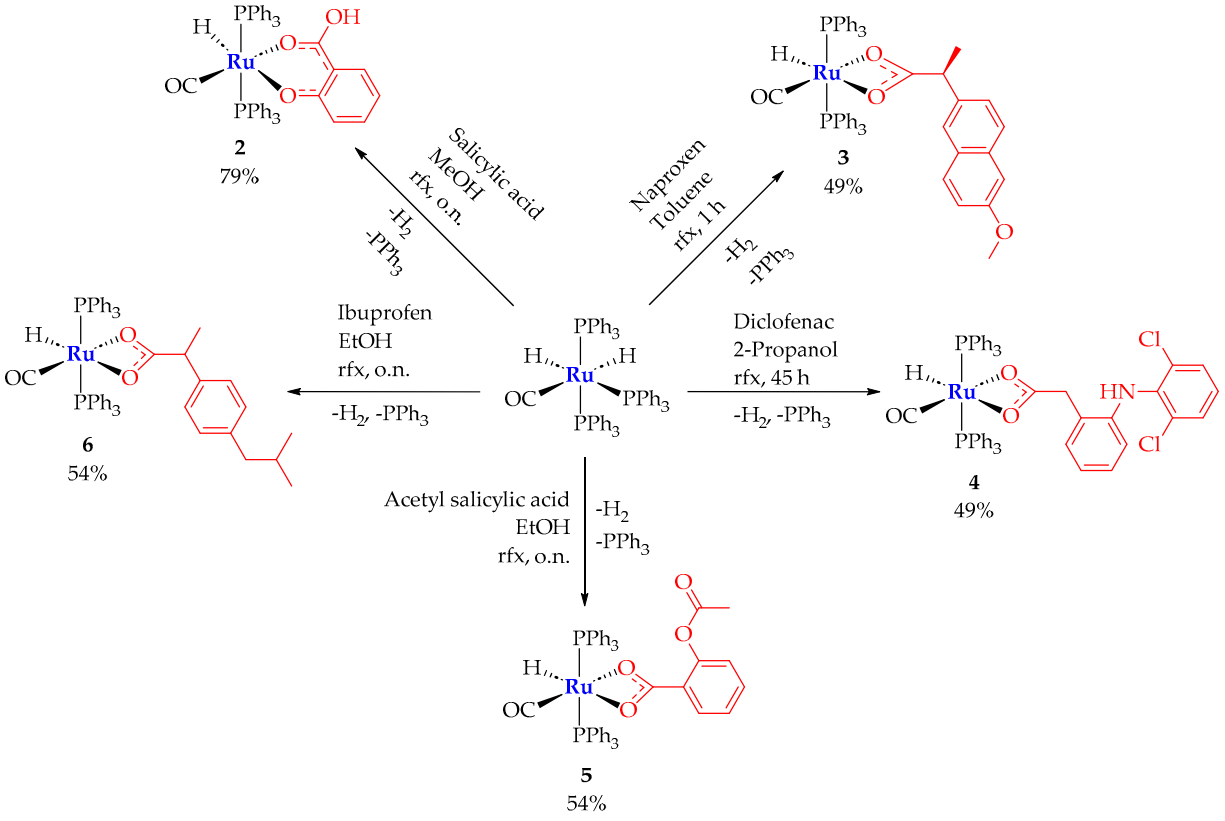

Scheme 1. Synthetic pathways and percentage yields for complexes **2**–**6**. All the products share the general formula [RuH(CO)(PPh_3)$_2$(NSAID)]. In the scheme, o.n. is used as an abbreviation for overnight.

2.1. Infrared Spectroscopy

IR spectral analyses are in agreement with the proposed structures. The IR spectra of **3**–**6** demonstrate asymmetric carboxy absorptions in the 1634–1521 cm^{-1} interval, close to the lower frequency set of bands (1526–1455 cm^{-1}) attributable to the symmetric stretching. These signals are diagnostic for a dihapto coordination mode that allows the formation of four-membered metallacycles. An intermolecular H-bond network can be invoked, promoted by aryl-substituent lone pairs, such as those from hydroxyl or methoxy groups in the salicylate class of ligands, as well as the chloride in coordinated diclofenac. In the case of complex **2** (Scheme 1), the coordination of the salicylate ligand is supported by the occurrence of an OH stretching band. Useful comparisons are provided in Table 1.

Table 1. Selected bands observed in FTIR spectra of complexes **2**–**6**. Wavenumbers are reported in cm^{-1}.

Entry	Name	Formula	ν (CH)ar	ν (Ru-H)	ν (C≡O)	ν (COO)
2	Ru–Salicylic acid	$[RuH(CO)(PPh_3)_2(Sal)]$	3053, vw	2001, w	1927, s	*asym* 1533, w; *sym* 1332, w
3	Ru–Naproxen	$[RuH(CO)(PPh_3)_2(Nap)]$	3055, w	Overlapped	1923, s	*asym* 1634, w; *sym* 1526, m
4	Ru–Diclofenac	$[RuH(CO)(PPh_3)_2(Dicl)]$	3053, vw	2078, w	1915, s	*asym* 1557, m; *sym* 1455, m
5	Ru–Acetylsalicylic acid	$[RuH(CO)(PPh_3)_2(MeOSal)]$	3056, vw	2011, w	1909, s	*asym* 1571, w; *sym* 1465, m
6	Ru–Ibuprofen	$[RuH(CO)(PPh_3)_2(Ibu)]$	3056, w	1995, w	1924, s	*asym* 1521, m; *sym* 1458, m

2.2. NMR Spectra of the Prepared Complexes

^1H, $^{31}P\{^1H\}$, $^{13}C\{^1H\}$, and bidimensional COSY, HSQC, and HMBC NMR spectra support the predicted molecular structure for complexes **2**–**6**. Multiplets in the range of 7.64–7.14 ppm demonstrate the presence of two triphenylphosphine ligands. In the precursor spectrum, two ^1H NMR signals are observed at −6.50 and −8.30 ppm, respectively. These are attributed to the highly shifted hydride ligands, whereas single hydride triplets are observed in the range −16.33/−16.91 ppm in the spectra of complexes **2**–**6**, due to the coupling with the equivalent trans-PPh_3, as confirmed by the $^{31}P\{^1H\}$ NMR resonances in the 43.09–44.60 ppm interval. The ^{13}C NMR spectra of **2**–**6** display a downfield triplet at about 205 ppm, assigned to Ru-CO, while the singlets of the carboxylic carbon atoms fall in the range 186.05–178.53 ppm (Table 2).

Table 2. Color, yield (%), and spectroscopical data of **2**–**6**. Chemical shifts are reported in ppm and UV–Vis absorptions in nm.

Entry	Name	Color	Yield	NMR			UV–Vis
				^1H-RuH	$^{31}P\{^1H\}$–PPh_3	$^{13}C\{^1H\}$–Ru(CO)	λ_{max}
2	Ru–Salicylic acid	Grey	79	−16.91	43.09	205.09	261
3	Ru–Naproxen	Red	49	−16.45	43.29	205.54	260
4	Ru–Diclofenac	Grey	49	−16.62	44.55	205.36	275
5	Ru–Acetylsalicylic acid	Grey	54	−16.32	44.58	205.48	274
6	Ru–Ibuprofen	White	53	−16.44	43.30	205.59	259

2.3. ESI-MS and UV Spectra

Mass spectrometry provides fundamental information regarding the structure of complexes in solution. In the ESI-MS spectra of complexes **2** to **6**, acquired in MeCN, the most relevant peak is the one related to the $[M–H]^+$ composition. Other common fragments detected are $[M–H + MeCN]^+$, $[M–L + 2\ MeCN]^+$, $[M–L + MeCN]^+$, and $[M–L]^+$ (where L is the coordinated NSAID ligand). The latter appears as a high-intensity peak, and it is related to the loss of O-donor ligands, confirming major metal affinity for softer carbonyl and triphenylphosphine ligands. The carboxylate coordinative mode of the NSAID's dihapto k^2-species indicates displacement by the acetonitrile solvent used in the ESI-MS technique, since MeCN shows softer and more nucleophilic aptitude compared to the delocalized k^2-C(O)O moiety, typical of all NSAID ligands. In the absence of mechanistic studies, it would be difficult to confirm the integrity of the metal organometallic structure along the targeted path. Isotopic peak patterns are all in good agreement with the simulated spectra.

The UV–Vis spectra of the complexes have been acquired in DMSO solution. A band in the range 259–275 nm has been observed in the analyzed species (Table 2) and attributed to intra-ligand charge transfer transition (ILCT). All recorded spectra are shown in Supplementary Information (Figures S7, S16, S24, S32 and S41).

2.4. Description of the X-Ray Crystal Structures of **4** and **5**

X-ray-quality crystals of **4** and **5** were grown by a double-layer crystallization technique (DCM-hexane = 1:10), and their structures were determined using Single Crystal X

Ray Diffraction (SCXRD). In both structures, the ruthenium atom adopts a distorted octahedral geometry in which the PPh_3 ligands are in a mutual *trans*-position (Figure 4a,b) and one hydride, one carbonyl, and one carboxylate ligand occupy equatorial coordination sites. The molecular structure of **4** shows an asymmetric chelate coordination of the carboxyl group of the diclofenac ligand [Ru-O1 2.183(2) and Ru-O2 2.310(2) Å, respectively]. This is presumably due to the presence of the very bulky substituent (2,6-dichlorophenylamine) in the *ortho*-position of the benzyl ring, which is on the same side as O2. In addition, the conformation of the coordinated diclofenac ligand shows some differences compared to that found in the crystal structure of the diclofenac acid [37], with the dihedral angle between the least-squares planes of the two aromatic rings being wider in the latter. Another significant effect attributable to steric crowding is the deviation from linearity of the P-Ru-P angle [171.94(3)°], which relieves the steric strain between the phenyl groups of the axial phosphines and the bulky diclofenac ligand. The two Ru-P distances are almost identical [Ru-P 2.3455(8) and 2.3458(9) Å]. Intramolecular hydrogen bonds in the diclofenac ligand also play an important role: in fact, the carboxylic oxygen O2 is involved in both classical [NH. . .O2] and nonclassical hydrogen bonds [C23H23. . .O2 and C45H45. . .O2] with one phenyl ring from the two PPh_3 ligands, the most significant being the NH. . .O2 interaction [N1. . .O2 2.904(4) Å and N1-H1N. . .O2 150°]. In the crystal packing, intermolecular H bonds are established through one of the two chlorine atoms (Cl2) and one H atom of the methylene moiety of the diclofenac belonging to adjacent molecules, thus forming dimeric units (Figure S41). Furthermore, an important role is played by π–π interactions between two 2,6-dichlorophenyl rings [centroid–centroid distance 3.555 Å] of neighboring molecules, generating dimers (Figure S42) different from the ones generated by H bonds. To the best of our knowledge, very few ruthenium complexes bearing the diclofenac ligand coordinated in a chelate fashion have been crystallographically investigated [38].

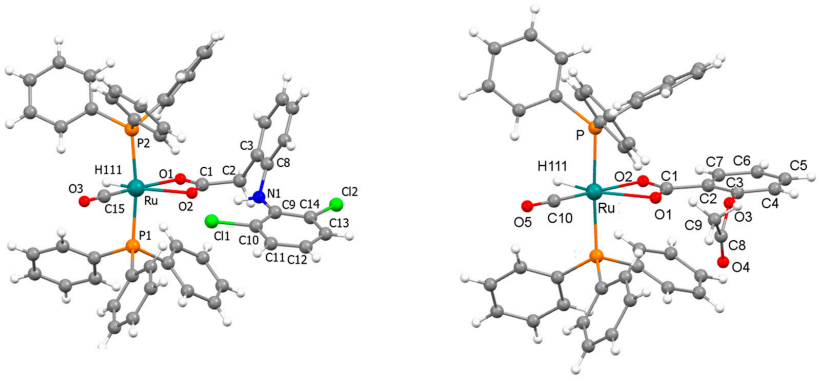

(**a**) (**b**)

Figure 4. Single crystal structures of complexes **4** (**a**) and **5** (**b**).

In the crystal structure of **5**, the Ru atom, the hydride, the CO, and most of the chelating acetylsalicylate ligand lie on a crystallographically imposed symmetry plane. This symmetry is broken by the carbonyl [C8 and O4] of the acetylsalicylate AcO group that is disordered over two positions below and above the aromatic ring plane with half occupancy. Also, in complex **5**, the two Ru-O distances are significantly different [Ru-O1 2.318(5) and Ru-O2 2.165(5) Å], while the Ru-P distance [2.353(1) Å] is almost identical to those reported for **4**. The asymmetry in the carboxylate coordination is likely caused by steric hindrance, as the weaker Ru-O interaction involves O1, which is located in the *ortho*-position and on the same side as the bulky AcO- substituent. In the crystal packing of **5**, in addition to intramolecular H bonds, nonclassical intermolecular H bonds [C24-H24. . .O1, C6-H6. . .O2] are at work (Figure S43).

2.5. Stability of the Tested Complexes

None of the complexes is moisture sensitive. The salicylic acid–Ru **2** complex is slightly air sensitive.

2.5.1. Stability in Aqueous Solution of **2**

A preliminary evaluation of the antiproliferative properties shown by complex **2** was performed using the MTT assay. Prior to that, the stability in solution was evaluated by recording UV–Vis spectra in phosphate-buffered solution (PBS-5% DMSO, pH 7.4) over a period of 48 h. The spectra showed no wavelength shifts, indicating preserved structural integrity throughout the experiment duration (Figure S8, Supplementary Material).

2.5.2. Stability of **6**

The stability of complex **6** was evaluated by the ^{1}H NMR spectroscopy in $CDCl_3$ solution observed over 48 h, confirming both the chemical shift position and invariant shape of the equivalent Me group signals of the isobutyl unit (0.84 ppm) and the distinct $\alpha-$carboxylic Me unit (0.53 ppm).

2.6. Antiproliferative Activity of **2** *and* **6**

The anticancer ability of the ruthenium complexes **2** and **6** was evaluated using an MTT proliferation assay for HeLa cells. Dose–response graphs were constructed to determine the IC_{50} concentrations of various treatments, and the results are shown in Figure 5A,B. Complex **6** shows no toxic activity at any of the concentrations tested, thus confirming that cytotoxicity is heavily dependent on the coordinated NSAID. In contrast, complex **2** shows an IC_{50} of 75.0 ± 0.8 μM, although it is less efficient than the *cis*-platin results in analogous conditions (12.3 μM) [39]. Interestingly, compound **2** shows an antiproliferative effect already at a concentration of 20 μM, reducing cell growth by 18.8 ± 5.8%. The in vitro antiproliferative properties of **2** are in line with those of other reported NSAID–ruthenium complexes [20,38].

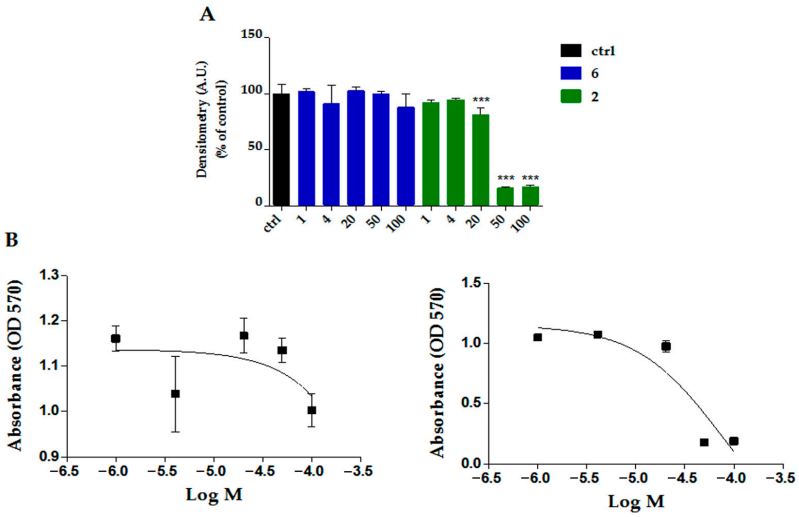

Figure 5. Viability of HeLa cells in the presence of different concentrations of the compounds. (**A**) The cells were treated for 48 h with a concentration range of (1–100 μM) with compounds **2** or **6** dissolved in DMSO. Data are reported as the percentages of viable cells ± SDs of three independent measurements in comparison to the vehicle control (DMSO). The statistical analysis was performed using a one-way analysis of variance test (*** $p < 0.001$). Cell viability was determined by the MTT assay, as described in the Materials and Methods Section. (**B**) Dose–response curves of HeLa cell viability upon treatment with different concentrations of (left) **6** and (right) **2**.

In all cases, the NSAID ligands coordinate via oxygen atoms of the carboxylate groups, except for salicylate in complex **2**, which anchors the carbonyl unit together with the phenolate group. Despite the difference shown in the coordination mode, remarkable bioactivity may suggest that pharmacokinetic pathways could be similar to those evidenced by the analogous buffered aspirin derivative [40].

3. Materials and Methods

3.1. General

All the Ru–hydride adducts with NSAIDs were obtained using the analogous procedure by optimizing the synthesis through the selection of the solvent so that the obtained adducts are insoluble. This triggers an almost complete selective precipitation, avoiding undesirable side or subsequent reaction pathways. The yield of complexes **3**–**6** is ca. 50%. Under the reaction conditions, conversion goes to completion only upon thermal activation; therefore, the formed coproducts are difficult to analyze because of adsorption on the solid stationary phase during chromatography in the purification procedure.

NMR measurements were taken at 298 K on a Mercury Plus 400 instrument (Oxford Instruments, Abingdon-on-Thames, UK). Frequencies are reported in Hz, and the chemical shifts are referenced to the solvent. The chemical shifts are expressed in parts per million (ppm). The multiplet lists are reported with the aid of two-dimensional COSY, HSQC, and HMBC NMR spectra. All the chemicals were of reagent grade and were used as received from commercial suppliers. Commercially available [$RuCl_3 \cdot xH_2O$] was purchased from Strem (Bischheim, France).

Elemental analyses were performed using a Thermo Fischer Scientific Flash 2000 CHNS instrument (Walter, MA, USA). In the elemental analyses (E, %), the small discrepancies are likely due to traces of adsorbed solvents in the microcrystalline powders.

Infrared spectra (4000–400 cm^{-1}) were recorded at 298 K on a PerkinElmer Spectrum 2000 Ftir (Fourier transform infrared) spectrophotometer (Waltham, MA, USA), and ESI-MS (electrospray ionization mass spectrometry) spectra were recorded on a Waters Micromass ZQ 4000 (Milford, MA, USA), with samples dissolved in MeCN. The spectra acquired for the powders were compared to those obtained for the crystals, and no significant differences were observed.

3.2. Synthesis of Ru–Salicylic Acid Complex **2**

A small excess of salicylic acid (37 mg, 0.268 mmol) and [$Ru(H)_2(CO)(PPh_3)_3$] **1** (220 mg, 0.240 mmol) were dissolved in methanol (15 mL) and refluxed overnight. Upon cooling to room temperature, a grey powder precipitate formed. The solid was then filtered and washed with methanol (3 mL aliquots for 3 times), then dried under vacuum.

Yield: 79%. Elemental analysis (%) Calc. for $RuC_{44}H_{36}P_2O_4$ Found (calc): C: 65.61 (65.75); H: 4.61 (4.58). ATR-FTIR (ν, cm^{-1}): 3053 (aromatic CH), 2001 (RuH), 1927 (C≡O), 1625 (COOH), 1598 (C=C-C), 1464 (C=C-C), 1432 (CH, PPh_3), 1254 (C-O), 1095 (PPh). ^1H NMR (400 MHz, $CDCl_3$) (δ, ppm) 10.59 (1H, COOH, s), 7.53–7.30 (30H, PPh_3, m), 7.05 (1H, C-H, m), 7.03 (1H, C-H, m), 6.53 (1H, C-H, dd), 6.45 (1H, C-H, dt), −16.91 (1H, Ru-H, t, $^2J_{H-P}$ = 20.04 Hz), ^{13}C NMR (101 MHz, $CDCl_3$) (δ, ppm): 205.24 (Ru-C≡O, t), 178.53 (COOH), 159.81 (C-H), 133.08 (PPh_3), 133.05 (C-H), 129.97 (PPh_3), 129.79 (C-H), 128.25 (PPh_3), 117.52 (C-H), 116.03 (C-H), 115.91 (C-H). ^{31}P NMR (162 MHz, $CDCl_3$) (δ, ppm): 43.09 (2P, PPh_3). ESI-MS^+ (MeCN) (*m*/*z*): 791 $[M-H]^+$.

3.3. Synthesis of Ru–Naproxen Complex **3**

Naproxen (63 mg, 0.272 mmol) and [$Ru(H)_2(CO)(PPh_3)_3$] **1** (250 mg, 0.272 mmol) were dissolved in toluene (15 mL) and refluxed until the IR Ru-CO absorption of **1** at

1940 cm^{-1} disappeared. After 1 h, the mixture was cooled down to room temperature, and the solvent evaporated under vacuum. The powder was then dissolved in 1 mL of DCM, and hexane (15 mL) was added to precipitate a red powdered microcrystalline solid, which was then filtered, washed with hexane (3 times with 10 mL aliquots), and finally dried under vacuum.

Yield: 49%. Elemental analysis (%) Calc. for $RuC_{51}H_{44}P_2O_4$ Found (calc): C: 69.60 (69.30); H: 5.16 (5.02). ATR-FTIR (ν, cm^{-1}): 3055 (aromatic CH), 2929 (aliphatic CH), 1923 (C≡O), 1634 (asym. COO), 1606 (C=C-C), 1526 (asym. COO), 1455 (C=C-C), 1434 (CH, PPh_3), 1267 (C-O), 1095 (PPh). ^{1}H NMR (400 MHz, $CDCl_3$) (δ, ppm), 7.55–7.29 (30 H, PPh_3, m) 7.06–6.96 (5H, m), 6.60 (1H, CH, d), 3.90 (3H, OCH_3, s) 2.56 (1H, CH, q), 0.64 (3H, CH_3, d), −16.45 (1H, Ru-H, t, $^2J_{H-P}$ = 21.45 Hz). ^{13}C NMR (101 MHz, $CDCl_3$) (δ, ppm): 205.54 (Ru-C≡O), 185.84 (COO), 157.19 (CH), 134.41 (PPh_3), 133.89 (CH), 132.20 (PPh_3), 129.79 (PPh_3), 128.72 (CH), 128.59 (CH), 128.15 (PPh_3), 127.53 (CH), 127.22 (CH), 126.20 (CH), 118.15 (CH), 105.61 (CH), 55.41 (CH), 47.85 (CH_3), 17.89 (OCH_3). ^{31}P NMR (162 MHz, $CDCl_3$) (δ, ppm): 43.29 (2P, PPh_3). ESI-MS$^+$ (MeCN) (*m*/*z*): 883 $[M-H]^+$.

3.4. Synthesis of Ru–Diclofenac Complex **4**

A small excess of diclofenac (107 mg, 0.361 mmol) and $[Ru(H)_2(CO)(PPh_3)_3]$ **1** (276 mg, 0.301 mmol) were dissolved in 2-propanol (40 mL) and refluxed for 45 h. A grey powder precipitated by cooling down to room temperature. The solid was then filtered, washed with 2-propanol (3 mL aliquots × 3 times), and dried under vacuum.

Yield: 49%. Elemental analysis (%) Calc. for $RuC_{51}H_{40}P_2NO_3Cl_2$ Found (calc): C: 64.72 (64.56); H: 4.30 (4.25). ATR-FTIR (ν, cm^{-1}): 3263 (NH), 3053 (aromatic CH), 2079 (RuH), 1915(C≡O), 1578 (C=C-C), 1557 (asym. COO), 1455 (sym. COO), 1431 (CH, PPh_3), 1093 (PPh). ^{1}H NMR (400 MHz, $CDCl_3$) (δ, ppm), 7.64 (1H, NH, s), 7.44–7.14 (30 H, PPh3, m), 7.35 (1H, C-H, d), 6.96 (1H, CH, t), 6.87 (1H, CH, t), 6.52 (1H, CH, d), 6.32 (1H, CH, d), 6.24 (1H, CH, d), 2.51 (2H, CH_2, s), −16.69 (1H, Ru-H, t, $^2J_{H-P}$ = 20.3 Hz) ^{13}C NMR (101 MHz, $CDCl_3$) 205.41 (Ru-C≡O, t), 183.99 (COO), 142.83 (CH), 138.72 (CH), 134.34 (PPh_3), 133.33 (PPh_3), 130.46 (CH), 129.88 (PPh_3), 129.73 (CH), 128.90 (CH), 128.23 (PPh_3), 126.68 (CH), 125.09 (CH), 123.29 (CH), 120.97 (CH), 117.28 (CH), 41.57 (CH_2). ^{31}P NMR (162 MHz, $CDCl_3$) (δ, ppm): 44.60 (2P, PPh_3). ESI-MS$^+$ (MeCN) (*m*/*z*): 948 $[M-H]^+$.

3.5. Synthesis of Ru–Acetylsalicylic Acid Complex **5**

Acetylsalicylic acid (39 mg, 0.218 mmol) and $[Ru(H)_2(CO)(PPh_3)_3]$ **1** (220 mg, 0.218 mmol) were dissolved in ethanol (15 mL) and refluxed overnight. A grey powder precipitated after cooling down the mixture solution to room temperature. The obtained solid was then filtered, washed with ethanol (3 times with 3 mL aliquots), and dried under vacuum.

Yield: 54%. Elemental analysis (%) Calc. for $RuC_{46}H_{38}P_2O_5$ Found (calc): C: 66.42 (66.26); H: 4.62 (4.59). ATR-FTIR (ν, cm^{-1}): 3056 (aromatic CH), 2011 (RuH), 1909 (C≡O), 1761 ($COOCH_3$), 1587 (C=C-C), 1571 (asym. COO), 1465 (sym. COO), 1433 (CH, PPh_3), 1200 (C-O). ^{1}H NMR (400 MHz, $CDCl_3$) (δ, ppm) 7.54–7.30 (30 H, PPh_3), 7.16 (1 H, CH, dt), 7.05 (1 H, CH, dd), 6.84 (1H, CH, dt), 6.69 (1 H, CH, dd), 2.10 (3 H, CH_3, s), −16.32 (1 H, RuH, t, $^2J_{H-P}$ = 20.34 Hz), ^{13}C NMR (101 MHz, $CDCl_3$) (δ, ppm): 205.64 (C≡O), 185.08 (COO), 175.02 ($C(O)OCH_3$), 169.55 (C-O), 149.82 (C), 134.79 (PPh_3), 133.50 (PPh_3), 131.62 (CH), 131.50 (CH), 129.78 (PPh_3), 129.15 (PPh_3), 124.57 (CH), 122.75 (CH), 21.29 (CH_3). ^{31}P NMR (162 MHz, $CDCl_3$) (δ, ppm): 44.58 (2P, PPh_3). ESI-MS$^+$ (MeCN) (*m*/*z*): 833 $[M-H]^+$.

3.6. Synthesis of Ru–Ibuprofen Complex **6**

A small excess of ibuprofen (31 mg, 0.150 mmol) was dissolved in EtOH (40 mL) solution of $Ru(H)_2(CO)(PPh_3)_3]$ **1** (113 mg, 0.123 mmol) and refluxed overnight. The

cooling down to room temperature caused white powder precipitation. The solid was filtered, washed with hexane, and subsequently with H_2O (10 mL aliquots × 3 times). The obtained powder was dried under vacuum.

Yield: 53%. Elemental analysis (%) Calc. for $RuC_{50}H_{48}P_2O_3$ Found (calc): C: 70.01 (69.84); H: 5.70 (5.63). ATR-FTIR (ν, cm^{-1}): 3056 (aromatic CH stretch), 2955 (aliphatic CH stretch), 2867 (aliphatic CH stretch), 1995 (Ru-H), 1924 (C≡O), 1521 (asym. COO), 1480 (C=C-C), 1458 (sym. COO), 1432 (CH, PPh_3), (PPh), 1095 (PPh). ^{1}H NMR (400 MHz, $CDCl_3$) (δ, ppm): 7.45–7.30 (30 H, PPh_3, m), 6.69 (2 H, CH, d), 6.40 (2 H, CH, d), 2.41 (1 H, CH, q), 2.32 (2 H, CH_2, d), 1.75 (1 H, CH, dt), 0.84 (6 H, CH_3, dd), 0.53 (3 H, CH_3, d), −16.44 (1 H, Ru-H, t, $^2J_{H-P}$ = 21.00 Hz). ^{13}C NMR (101 MHz, $CDCl_3$) (δ, ppm): 205.59 (C≡O), 186.05 (COO), 139.00 (C), 138.92 (C), 134.44 (PPh_3), 133.91 (PPh_3), 129.79 (PPh_3), 128.64 (CH), 128.18 (PPh_3), 127.56 (CH), 47.61 (CH), 45.23 (CH_2), 30.31 (CH), 22.61 (CH_3), 17.90 (CH_3). ^{31}P NMR (162 MHz, $CDCl_3$) (δ, ppm): 43.30 (2P, PPh_3). ESI-MS$^+$ (MeCN) (m/z): 859 $[M-H]^+$.

3.7. X-Ray Crystallography

The X-ray intensity data for **4** and **5** were collected on a Bruker APEX CCD diffractometer (Bruker, Karlsruhe, Germany) using Mo−Kα or Cu-Kα radiation (for **5**). All data were processed using the Bruker suite of programs [41–43], and the structures were solved with SHELXT [44] and refined with the SHELXL programs [45]. All non-hydrogen atoms were assigned to anisotropic displacement parameters. Most of the hydrogen atoms were located in the Fourier map, placed in idealized positions, and included as riding with constrained isotropic displacement parameters for the aromatic and methyl protons and refined as riding with Uiso(H) = 1.2Ueq(C) or Uiso(H) = 1.3Ueq(C)methyl. Molecular graphics were generated using the program Mercury [46]. Table S1 reports crystal data and refinement parameters for **4** and **5**.

3.8. MTT Assay

HeLa Cells were purchased from American Type Culture Collection (ATCC, Manassas, VA, USA). Cells were seeded at 1.5 × 10^4 cells/well in a 96-well plastic culture plate (Sarstedt, Milan, Italy), and after 24 h of growth, were exposed to increasing concentrations of each distinct compound (from 0.25 μM to 10 μM) solubilized in RPMI 1640 medium. Cells were treated with DMSO (vehicle control). For the CDDP, the cells were treated at the same concentration range as the complexes. Treatments were left for 48 h to ensure efficient cellular uptake.

The MTT assay was performed according to the literature [47]. The absorbance at 570 nm was measured using a multiwell plate reader (Tecan, Männedorf, Switzerland), and data were analyzed by Prism GraphPad 8 software. Percent cell viability was determined with respect to the control. All concentrations were tested in triplicate, and the experiment was repeated three times.

4. Conclusions

Metal coordination aims to combine the anti-inflammatory effects of NSAIDs with the anticancer activities of the Ru species, potentially leading to novel synergistic therapeutic effects. The synthesized compounds contain both carboxylic groups from NSAIDs and phosphine ligands, therefore imparting amphiphilic features to the Ru core and enhancing its ability to be delivered to cancer targets. Herein, we report ruthenium complexes coordinating four non-steroidal anti-inflammatory drugs (NSAIDs) and the salicylate moiety as an aspirin precursor, which have been synthesized and spectroscopically and structurally investigated. The rationale for the synthesis of novel Ru–NSAID complexes

consists of providing pharmacophore molecules for targeting cancer, while the ruthenium central core might provide further cytotoxic features, such as DNA binding to trigger apoptosis via ROS mediation [16,20,38].

The MTT assay on HeLa cancer cells performed with salicylic complex **2** suggests antiproliferative activity, albeit at relatively elevated doses. Future perspectives include extending investigations to additional biological targets, such as interaction measures with human serum albumin, calf-thymus DNA, and iron-carrier protein transferrin. In summary, we believe that Ru coordination is responsible for promoting synergistic effects by integrating complementary advantages, leading to improved tumor targeting and therapeutic outcomes by minimizing systemic toxicity, analogous to the findings in the case of small molecule–drug conjugates [48–50].

To address pharmacological resistance and toxic effects, novel therapeutics aim to enhance selectivity by penetrating exclusively into cancer cells while exhibiting steady and durable efficacy with minimal administered doses. However, many issues have yet to be overcome to allow Ru species to be tested as therapeutics in the next clinical phases. Aiming at this ambitious health target, it would be aspirational, for instance, to improve both the hydrolysis and metabolic absorption features of future synthesized Ru species [28].

Supplementary Materials: The following supporting information can be downloaded at https://www.mdpi.com/article/10.3390/molecules31040589/s1, Characterization of complexes: Figures S1–S43; Stability assessment of **2** through UV spectroscopy: Figure S8; Stability assessment of **6** through ^{1}H NMR spectroscopy: Figure S36; X-ray diffraction studies: Table S1, Figures S42 and S43.

Author Contributions: Conceptualization, S.B.; data curation, M.M., G.D., and F.M.; formal analysis, M.M.; funding acquisition, S.B.; investigation, G.D., and M.M.; methodology, S.B., G.D., and C.B.; project administration, S.B.; resources, S.B., M.M., and C.B.; supervision, S.B.; validation, S.B., and C.B.; writing—original draft, S.B., G.D., and F.M.; writing—review and editing, S.B., M.M., and F.M. All authors have read and agreed to the published version of the manuscript.

Funding: This research was funded by Alma Mater Studiorum-Università di Bologna grant RFO 2023 (to S.B.).

Institutional Review Board Statement: Not applicable.

Informed Consent Statement: Not applicable.

Data Availability Statement: The original contributions presented in the study are included in the article/Supplementary Material; further inquiries can be directed to the corresponding authors.

Acknowledgments: We are deeply grateful to Natalia Calonghi for offering her expertise and teaching G.D. to perform biological MTT assays. Her dedication and meticulous attention to detail significantly contributed to the quality and success of this research. We are also thankful to Cristiano Valli for providing some data during his Master's thesis.

Conflicts of Interest: The authors declare no conflicts of interest.

References

1. Han Ang, W.; Dyson, P.J. Classical and Non-Classical Ruthenium-Based Anticancer Drugs: Towards Targeted Chemotherapy. *Eur. J. Inorg. Chem.* **2006**, *2006*, 4003–4018. [CrossRef]
2. Bratsos, I.; Jedner, S.; Gianferrara, T.; Alessio, E. Ruthenium Anticancer Compounds: Challenges and Expectations. *Chimia* **2007**, *61*, 692. [CrossRef]
3. Kavukcu, S.B.; Özverel, C.S.; Kıyak, N.; Vatansever, H.S.; Türkmen, H. Ruthenium Compounds: Are They the next-Era Anticancer Agents? *Appl. Organomet. Chem.* **2024**, *38*, e7363. [CrossRef]
4. Lee, S.Y.; Kim, C.Y.; Nam, T.-G. Ruthenium Complexes as Anticancer Agents: A Brief History and Perspectives. *Drug Des. Dev. Ther.* **2020**, *14*, 5375–5392. [CrossRef]

5. Coverdale, J.P.C.; Laroiya-McCarron, T.; Romero-Canelón, I. Designing Ruthenium Anticancer Drugs: What Have We Learnt from the Key Drug Candidates? *Inorganics* **2019**, *7*, 31. [CrossRef]
6. Zeng, L.; Gupta, P.; Chen, Y.; Wang, E.; Ji, L.; Chao, H.; Chen, Z.-S. The Development of Anticancer Ruthenium(II) Complexes: From Single Molecule Compounds to Nanomaterials. *Chem. Soc. Rev.* **2017**, *46*, 5771–5804. [CrossRef]
7. Tang, X.; Liang, X. Metal-Mediated Targeting in the Body. *Chem. Biol. Drug Des.* **2013**, *81*, 311–322. [CrossRef]
8. Ali, N.W.; Gamal, M.; Abdelkawy, M. Simultaneous Determination of Hyoscine N-Butyl Bromide and Paracetamol in Their Binary Mixture by RP-HPLC Method. *Arab. J. Chem.* **2017**, *10*, S1868–S1874. [CrossRef]
9. Starek, M.; Krzek, J. A Review of Analytical Techniques for Determination of Oxicams, Nimesulide and Nabumetone. *Talanta* **2009**, *77*, 925–942. [CrossRef]
10. Banti, C.N.; Hadjikakou, S.K. Non-Steroidal Anti-Inflammatory Drugs (NSAIDs) in Metal Complexes and Their Effect at the Cellular Level. *Eur. J. Inorg. Chem.* **2016**, *2016*, 3048–3071. [CrossRef]
11. Cuzick, J.; Otto, F.; Baron, J.A.; Brown, P.H.; Burn, J.; Greenwald, P.; Jankowski, J.; Vecchia, C.L.; Meyskens, F.; Senn, H.J.; et al. Aspirin and Non-Steroidal Anti-Inflammatory Drugs for Cancer Prevention: An International Consensus Statement. *Lancet Oncol.* **2009**, *10*, 501–507. [CrossRef]
12. Czapski, G.A.; Czubowicz, K.; Strosznajder, J.B.; Strosznajder, R.P. The Lipoxygenases: Their Regulation and Implication in Alzheimer's Disease. *Neurochem Res* **2016**, *41*, 243–257. [CrossRef]
13. Kostova, I. Rational Design of Metal-Based Pharmacologically Active Compounds. *Inorganics* **2024**, *12*, 335. [CrossRef]
14. Lucaciu Stan, R.; Hangan, A.; Sevastre, B.; Oprean, L. Metallo-Drugs in Cancer Therapy: Past, Present and Future. *Molecules* **2022**, *27*, 6485. [CrossRef]
15. Martling, A.; Hed Myrberg, I.; Nilbert, M.; Grönberg, H.; Granath, F.; Eklund, M.; Öresland, T.; Iversen, L.H.; Haapamäki, C.; Janson, M.; et al. Low-Dose Aspirin for PI3K-Altered Localized Colorectal Cancer. *N. Engl. J. Med.* **2025**, *393*, 1051–1064. [CrossRef] [PubMed]
16. Oliveira, K.M.; Honorato, J.; Gonçalves, G.R.; Cominetti, M.R.; Batista, A.A.; Correa, R.S. Ru(II)/Diclofenac-Based Complexes: DNA, BSA Interaction and Their Anticancer Evaluation against Lung and Breast Tumor Cells. *Dalton Trans.* **2020**, *49*, 12643–12652. [CrossRef]
17. Sáez, R.; Lorenzo, J.; Prieto, M.J.; Font-Bardia, M.; Calvet, T.; Omeñaca, N.; Vilaseca, M.; Moreno, V. Influence of PPh3 Moiety in the Anticancer Activity of New Organometallic Ruthenium Complexes. *J. Inorg. Biochem.* **2014**, *136*, 1–12. [CrossRef]
18. Aman, F.; Hanif, M.; Siddiqui, W.A.; Ashraf, A.; Filak, L.K.; Reynisson, J.; Söhnel, T.; Jamieson, S.M.F.; Hartinger, C.G. Anticancer Ruthenium(η^6-*p*-Cymene) Complexes of Nonsteroidal Anti-Inflammatory Drug Derivatives. *Organometallics* **2014**, *33*, 5546–5553. [CrossRef]
19. Ahmad Khan, R.; Al-Lohedan, H.A.; Abul Farah, M.; Sajid Ali, M.; Alsalme, A.; Mashay Al-Anazi, K.; Tabassum, S. Evaluation of (η^6-*p*-Cymene) Ruthenium Diclofenac Complex as Anticancer Chemotherapeutic Agent: Interaction with Biomolecules, Cytotoxicity Assays. *J. Biomol. Struct. Dyn.* **2019**, *37*, 3905–3913. [CrossRef]
20. Srivastava, P.; Mishra, R.; Verma, M.; Sivakumar, S.; Patra, A.K. Cytotoxic Ruthenium(II) Polypyridyl Complexes with Naproxen as NSAID: Synthesis, Biological Interactions and Antioxidant Activity. *Polyhedron* **2019**, *172*, 132–140. [CrossRef]
21. Mandal, P.; Kundu, B.K.; Vyas, K.; Sabu, V.; Helen, A.; Dhankhar, S.S.; Nagaraja, C.M.; Bhattacherjee, D.; Bhabak, K.P.; Mukhopadhyay, S. Ruthenium(II) Arene NSAID Complexes: Inhibition of Cyclooxygenase and Antiproliferative Activity against Cancer Cell Lines. *Dalton Trans.* **2018**, *47*, 517–527. [CrossRef] [PubMed]
22. Benadiba, M.; de M. Costa, I.; Santos, R.L.S.R.; Serachi, F.O.; De Oliveira Silva, D.; Colquhoun, A. Growth Inhibitory Effects of the Diruthenium-Ibuprofen Compound, [$Ru_2Cl(Ibp)_4$], in Human Glioma Cells in Vitro and in the Rat C6 Orthotopic Glioma in vivo. *J. Biol. Inorg. Chem.* **2014**, *19*, 1025–1035. [CrossRef] [PubMed]
23. Sumithaa, C.; Ganeshpandian, M. Half-Sandwich Ruthenium Arene Complexes Bearing Clinically Approved Drugs as Ligands: The Importance of Metal–Drug Synergism in Metallodrug Design. *Mol. Pharm.* **2023**, *20*, 1453–1479. [CrossRef]
24. Golbaghi, G.; Castonguay, A. Rationally Designed Ruthenium Complexes for Breast Cancer Therapy. *Molecules* **2020**, *25*, 265. [CrossRef]
25. Graminha, A.E.; Popolin, C.; Honorato de Araujo-Neto, J.; Correa, R.S.; de Oliveira, K.M.; Godoy, L.R.; Vegas, L.C.; Ellena, J.; Batista, A.A.; Cominetti, M.R. New Ruthenium Complexes Containing Salicylic Acid and Derivatives Induce Triple-Negative Tumor Cell Death via the Intrinsic Apoptotic Pathway. *Eur. J. Med. Chem.* **2022**, *243*, 114772. [CrossRef]
26. Campideli, V.C.; Montilla-Suárez, J.M.; Silva, T.A.; Sicupira, D.C.; Oliveira, K.M.; Correa, R.S. Exploring DNA-Interaction and Molecular Structure of Ruthenium/1,2-Bis-(Diphenylphosphino)Ethane)-Based Complex. *Eur. J. Chem.* **2023**, *14*, 193–201. [CrossRef]
27. Teixeira, T.; Palmeira-Mello, M.V.; Machado, P.H.; Moraes, C.A.F.; Pinto, C.; Costa, R.C.; Badaró, W.; Gomes Neto, J.A.; Ellena, J.; Vieira Rocha, F.; et al. Ru(II)-Fenamic-Based Complexes as Promising Human Ovarian Antitumor Agents: DNA Interaction, Cellular Uptake, and Three-Dimensional Spheroid Models. *Inorg. Chem.* **2025**, *64*, 3707–3718. [CrossRef]

28. Dong-Ling, K.; Ka-Kit, L.; Lai-Hon, C.; Jun, H.; Chun-Yuen, W. Overview of Some Second- and Third-Row Late Transition Metal Pincer-Type N-Heterocyclic Carbene Complexes: Synthesis, Optical Properties, and Applications. *Molecules* **2025**, *30*, 2640. Available online: https://www.mdpi.com/1420-3049/30/12/2640 (accessed on 5 December 2025).
29. Amaya-Flórez, A.; R.-Galindo, J.; Sanchez-Yocue, E.; Ruiz-Martinez, A.; Serrano-García, J.S.; Romo-Pérez, A.; Cano-Sanchez, P.; Reyes-Marquez, V.; Lagadec, R.L.; Morales-Morales, D. Cyclometalated Complexes: Promising Metallodrugs in the Battle against Cancer. *RSC Med. Chem.* **2025**, *16*, 5125–5195. [CrossRef]
30. Tabrizi, L.; Olasunkanmi, L.O.; Fadare, O.A. Experimental and Theoretical Investigations of Cyclometalated Ruthenium(II) Complex Containing CCC-Pincer and Anti-Inflammatory Drugs as Ligands: Synthesis, Characterization, Inhibition of Cyclooxygenase and in Vitro Cytotoxicity Activities in Various Cancer Cell Lines. *Dalton Trans.* **2019**, *48*, 728–740. [CrossRef]
31. Correa, R.S.; De Oliveira, K.M.; Delolo, F.G.; Alvarez, A.; Mocelo, R.; Plutin, A.M.; Cominetti, M.R.; Castellano, E.E.; Batista, A.A. Ru(II)-Based Complexes with N-(Acyl)-N′,N′-(Disubstituted)Thiourea Ligands: Synthesis, Characterization, BSA- and DNA-Binding Studies of New Cytotoxic Agents against Lung and Prostate Tumour Cells. *J. Inorg. Biochem.* **2015**, *150*, 63–71. [CrossRef]
32. Hey, D.A.; Sauer, M.J.; Fischer, P.J.; Esslinger, E.-M.H.J.; Kühn, F.E.; Baratta, W. Acetate Acetylacetonate Ampy Ruthenium(II) Complexes as Efficient Catalysts for Ketone Transfer Hydrogenation. *ChemCatChem* **2020**, *12*, 3537–3544. [CrossRef]
33. Scott, D.C.; Clymer, J.W. Estimation of Distribution Coefficients from the Partition Coefficient and pKa. *Pharm. Technol.* **2002**, *26*, 30–40.
34. Boggara, M.B.; Krishnamoorti, R. Partitioning of Nonsteroidal Antiinflammatory Drugs in Lipid Membranes: A Molecular Dynamics Simulation Study. *Biophys. J.* **2010**, *98*, 586–595. [CrossRef]
35. Manrique-Moreno, M.; Heinbockel, L.; Suwalsky, M.; Garidel, P.; Brandenburg, K. Biophysical Study of the Non-Steroidal Anti-Inflammatory Drugs (NSAID) Ibuprofen, Naproxen and Diclofenac with Phosphatidylserine Bilayer Membranes. *Biochim. Biophys. Acta (BBA) Biomembr.* **2016**, *1858*, 2123–2131. [CrossRef] [PubMed]
36. Juračka, J.; Šrejber, M.; Melíková, M.; Bazgier, V.; Berka, K. MolMeDB: Molecules on Membranes Database. *Database* **2019**, *2019*, baz078. [CrossRef]
37. Pearson, R.G. Antisymbiosis and the Trans Effect. *Inorg. Chem.* **1973**, *12*, 712–713. [CrossRef]
38. Tadić, A.; Poljarević, J.; Krstić, M.; Kajzerberger, M.; Aranđelović, S.; Radulović, S.; Kakoulidou, C.; Papadopoulos, A.N.; Psomas, G.; Grgurić-Šipka, S. Ruthenium–Arene Complexes with NSAIDs: Synthesis, Characterization and Bioactivity. *New J. Chem.* **2018**, *42*, 3001–3019. [CrossRef]
39. Becit, M.; Aydın Dilsiz, S.; Başaran, N. Interaction of Curcumin on Cisplatin Cytotoxicity in HeLa and HepG2 Carcinoma Cells. *IJP* **2020**, *50*, 202–210. [CrossRef]
40. Chen, J.; Zhang, Y.; Jie, X.; She, J.; Dongye, G.; Zhong, Y.; Deng, Y.; Wang, J.; Guo, B.; Chen, L. Ruthenium(II) Salicylate Complexes Inducing ROS-Mediated Apoptosis by Targeting Thioredoxin Reductase. *J. Inorg. Biochem.* **2019**, *193*, 112–123. [CrossRef]
41. *APEX3 Software Package*, V2019; Bruker AXS Inc.: Madison, WI, USA, 2019.
42. *Bruker SAINT*, v8.40A; Part of the APEX3 Software Package V2019; Bruker AXS Inc.: Madison, WI, USA, 2019.
43. *Bruker SADABS*, V2016/2; Part of the APEX3 Software Package V2019; Bruker AXS Inc.: Madison, WI, USA, 2019.
44. Sheldrick, G. SHELXT—Integrated Space-Group and Crystal-Structure Determination. *Acta Crystallogr. Sect. A* **2015**, *71*, 3–8. [CrossRef] [PubMed]
45. Sheldrick, G.M. Crystal Structure Refinement with SHELXL. *Cryst. Struct. Commun.* **2015**, *71*, 3–8. [CrossRef]
46. Macrae, C.F.; Sovago, I.; Cottrell, S.J.; Galek, P.T.A.; McCabe, P.; Pidcock, E.; Platings, M.; Shields, G.P.; Stevens, J.S.; Towler, M.; et al. Mercury 4.0: From Visualization to Analysis, Design and Prediction. *J. Appl. Cryst.* **2020**, *53*, 226–235. [CrossRef] [PubMed]
47. Calonghi, N.; Farruggia, G.; Boga, C.; Micheletti, G.; Fini, E.; Romani, L.; Telese, D.; Faraci, E.; Bergamini, C.; Cerini, S.; et al. Root Extracts of Two Cultivars of Paeonia Species: Lipid Composition and Biological Effects on Different Cell Lines: Preliminary Results. *Molecules* **2021**, *26*, 655. [CrossRef] [PubMed]
48. Wang, X.; Guo, C.; Shao, J.; Zou, X.; Xing, S.; Xu, C.L.; Zhao, Q.; Wu, Y.; Sun, C.; Chen, Y.; et al. Small Molecule-Drug Conjugates: An Emerging Drug Design Strategy for Targeted Therapeutics. *J. Med. Chem.* **2025**, *68*, 24759–24784. [CrossRef]
49. Lerchen, H.-G.; Stelte-Ludwig, B.; Kopitz, C.; Heroult, M.; Zubov, D.; Willuda, J.; Schlange, T.; Kahnert, A.; Wong, H.; Izumi, R.; et al. A Small Molecule–Drug Conjugate (SMDC) Consisting of a Modified Camptothecin Payload Linked to an αVß3 Binder for the Treatment of Multiple Cancer Types. *Cancers* **2022**, *14*, 391. [CrossRef]
50. Meng, F.; Qi, T.; Liu, X.; Wang, Y.; Yu, J.; Lu, Z.; Cai, X.; Li, A.; Duan, J. 20P The Essential Role of DNA Repair in the Pharmacological Activities of AST-3424. *Ann. Oncol.* **2023**, *34*, S193. [CrossRef]